The Journal of Chemical Physics

RESEARCH ARTICLE | JANUARY 31 2024

Photoelectron velocity map imaging spectroscopy of group 14 elements and iron tetracarbonyl anionic clusters $MFe(CO)_4^-$ (M = Si, Ge, Sn)

Bangmin Ju; Ziheng Zhang; Xiangtao Kong ; Jinghan Zou ; Gang Li ; Hua Xie ; Ling Jiang

J. Chem. Phys. 160, 044307 (2024)
https://doi.org/10.1063/5.0187204

The Journal of Chemical Physics ARTICLE pubs.aip.org/aip/jcp

Photoelectron velocity map imaging spectroscopy of group 14 elements and iron tetracarbonyl anionic clusters $MFe(CO)_4^-$ (M = Si, Ge, Sn)

Cite as: J. Chem. Phys. 160, 044307 (2024); doi: 10.1063/5.0187204
Submitted: 12 November 2023 • Accepted: 9 January 2024 •
Published Online: 31 January 2024

Bangmin Ju,[1,2] Ziheng Zhang,[1] Xiangtao Kong,[3,a)] Jinghan Zou,[1] Gang Li,[1] Hua Xie,[1,a)] and Ling Jiang[1,a)]

AFFILIATIONS

[1] State Key Laboratory of Molecular Reaction Dynamics, Dalian Institute of Chemical Physics, Chinese Academy of Sciences, Dalian 116023, People's Republic of China

[2] University of Chinese Academy of Sciences, Beijing 100049, People's Republic of China

[3] Henan Key Laboratory of New Optoelectronic Functional Materials, College of Chemistry and Chemical Engineering, Anyang Normal University, Anyang 455000, People's Republic of China

[a)] **Authors to whom correspondence should be addressed:** kongxt@aynu.edu.cn; xiehua@dicp.ac.cn; and ljiang@dicp.ac.cn

ABSTRACT

The heteronuclear group 14 M-iron tetracarbonyl clusters $MFe(CO)_4^-$ (M = Si, Ge, Sn) anions have been generated in the gas phase by laser ablation of M–Fe alloys and detected by mass and photoelectron spectroscopy. With the support of quantum chemical calculations, the geometric and electronic structures of $MFe(CO)_4^-$ (M = Si, Ge, Sn) are elucidated, which shows that all the $MFe(CO)_4^-$ clusters have the M–Fe bonded, iron-centered, and carbonyl-terminal M–$Fe(CO)_4$ structure with the C_{2v} symmetry and a $^2B_2$ ground state. The M–Fe bond can be considered a double bond, which includes one σ electron sharing bond and one π dative bond. The C–O bonds in those anionic clusters are calculated to be elongated to different extents, and in particular, the C–O bonds in $SiFe(CO)_4^-$ are elongated more. The Si–Fe alloy thus turns out to be a better collocation to activate the C–O bonds in the gas phase among group 14. The present findings have important implications for the rational development of high-performance catalysts with isolated metal atoms/clusters dispersed on supports.

I. INTRODUCTION

Studies on metal carbonyl complexes are one of the most studied topics, given their unique chemical and catalytic characteristics.[1–9] Among the plentiful metal carbonyls, heteronuclear iron carbonyl clusters have aroused much interest since iron is frequently used as a component of catalysts. The studies on mass-selected gas-phase metal iron-carbonyl clusters can provide lots of information such as spectroscopic information, photophysical properties, and reaction kinetics, which are essential to understand the activation of CO on the surface of a metal as well as the binding properties at active sites of catalysts and could serve as examples to elucidate the detailed catalytic reaction mechanisms at the molecular level.[10–16] Furthermore, it could help to design and improve the activities of catalysts in the condensed phase.[5,17–20]

Since Mond's discovery of $Fe(CO)_5$ in 1891,[21] clusters with $Fe(CO)_n$ fragments have attracted more and more attention. The neutral iron carbonyl $Fe(CO)_5$ has a D_{3h} structure and fulfills the 18-electron rule, while the unsaturated metalloligand $Fe(CO)_4$ can be viewed as building blocks to form heteronuclear iron carbonyl complexes.[22–26] Recently, the M–Fe bonding feature in M–Fe tetracarbonyl clusters has been experimentally and theoretically studied. For example, the Mg–$Fe(CO)_4^-$ and Mg–Mg–$Fe(CO)_4^-$ clusters, in a doublet ground electronic state with the C_{3v} symmetry, both have electron-sharing Mg(I)–Fe(–II) σ bonds characterized by infrared photodissociation spectroscopy and quantum chemical calculations.[26] Similarly, the $CuFe(CO)_4^-$ and $AgFe(CO)_4^-$ clusters also have a σ bond with the C_{3v} structure.[22,23] In contrast, the $BeFe(CO)_4^-$ cluster has the triple Be–Fe bonding character, which includes one normal covalent bond and two weak Be ← $Fe(CO)_4^-$

dative π bonding.[24] In addition, the activation of CO ligands in $MFe(CO)_4^-$ clusters is also reported. For instance, the CO molecules are weakened in $MFe(CO)_4^-$ (M = Ti–Cr) complexes for the longer C–O bond distances (~1.18 Å) than that of the free CO molecule (1.13 Å) through photoelectron velocity map imaging spectroscopy and theoretical studies.[25] Further, the ScO^+ and YO^+ supported on $Fe(CO)_4^{2-}$ can oxidize CO to CO_2, in which $[Fe(CO)_4]^{2-}$ has dative bonding with MO^+.[27]

However, few attentions have been paid to heterobinuclear group 14-iron tetracarbonyl clusters $MFe(CO)_4^-$ (M = Si, Ge, Sn) in the gas phase so far. Here, we report the generation and photoelectron spectroscopic characterization of $MFe(CO)_4^-$ (M = Si, Ge, Sn). Density functional theory (DFT) calculations at the B3LYP/def2-TZVPP level were also conducted to obtain the geometrical and electronic structures. The combinations of experiments and computations show that $MFe(CO)_4^-$ clusters have a $^2B_2$ ground state with the C_{2v} symmetry. The M–Fe bonds are shown to be a double bond and the CO molecules in the three anionic clusters are activated to different extents.

II. EXPERIMENTAL AND COMPUTATIONAL METHODS

A. Experimental methods

The experiments were conducted by a homemade photoelectron spectroscopy instrument consisting of a Nd:YAG laser vaporization source, a dual-channel time-of-flight mass spectrometer, and a collinear photoelectron velocity map imaging spectrometer, of which the brief description is as follows, and details have been provided previously.[28] The heterobinuclear group 14 elements-iron tetracarbonyl clusters, $MFe(CO)_4^-$ (M = Si, Ge, Sn), were generated by 532 nm laser ablation to M–Fe (M = Si, Ge, Sn) alloy disks (mole ratio, M/Fe = 1:1), in a pulsed supersonic expansion of helium gas seeded with 5% CO at 2 atm backing pressure. The clusters, after cooling and supersonic expansion into the source chamber, were detected and mass-selected by the dual-channel time-of-flight mass spectrometer. Subsequently, the anions selected, were guided into the photodetachment region, where the photoelectrons were interacted with laser beams of 355 nm (3.496 eV) and detected by a microchannel plate/phosphor screen combination. The two-dimensional images on the phosphor screen were recorded by a CCD camera. Each image was obtained by accumulating 10 000–50 000 laser shots at a 10 Hz repetition rate. The photoelectron spectra (PES), reconstructed by the basis set expansion inverse Abel transform method (BASEX)[29] from raw images, were plotted vs the electron binding energy, which was acquired by subtracting the electron kinetic energy (eKE) from the detachment photon energy. The experimental photoelectron spectra are mainly discussed in the article. The spectrometer was calibrated by the known spectrum of Au^-, and the energy resolution was better than 5%, corresponding to 50 meV at an electron kinetic energy of 1 eV.

B. Computational methods

To analyze the PES images and confirm the geometrical and electronic structures of $MFe(CO)_4^-$ (M = Si, Ge, Sn) clusters, quantum chemical calculations by the density function theory (DFT) method were performed on the Gaussian 09 program.[30] In order to find the most appropriate computational level, the vertical detachment energy (VDE) for the most stable structure of $GeFe(CO)_4^-$ was predicted at different DFT levels (Table SI) and compared with the experimental data, and the B3LYP/def2-TZVPP method showed a good agreement between the calculated and experimental VDE values.[31–34] Then, all the calculations were carried out for the geometrical and electronic structures at the same level. Harmonic frequency analyses were performed to ensure that each structure was the real local minima on the potential energy surface. Quantum theory of atoms in molecular analyses was performed using the Multiwfn program.[35] Natural bond orbital (NBO) analyses were accomplished by using NBO 3.1[36] in the Gaussian 09 program.

III. RESULTS

A. Photoelectron image spectroscopy

The experimental photoelectron imaging spectra of $MFe(CO)_4^-$ (M = Si, Ge, Sn) clusters recorded at 355 nm are shown in Fig. 1. The 355 nm spectra made the observation of the ground-state transition of $MFe(CO)_4^-$ (M = Si, Ge, Sn) available, and the first dominant main peak in each spectrum is equal to the ground-state VDE of each species. As is shown in Fig. 1 and listed in Table I, the VDE values of $MFe(CO)_4^-$ (M = Si, Ge,

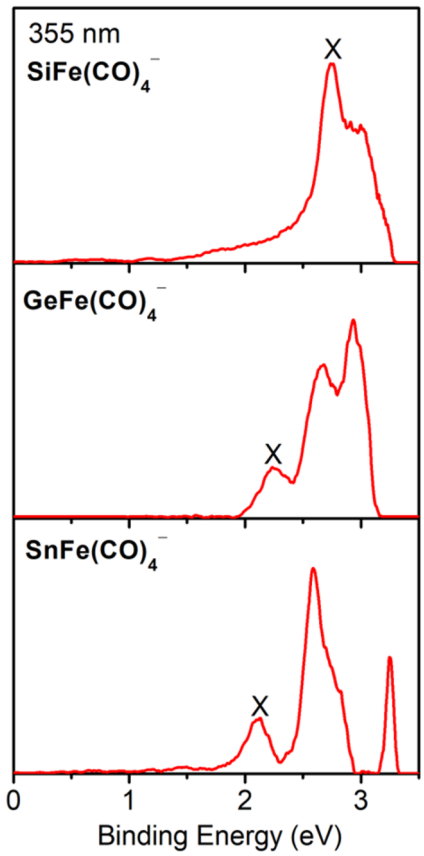

FIG. 1. Photoelectron spectra of $MFe(CO)_4^-$ (M = Si, Ge, Sn) at 355 nm (3.496 eV).

TABLE I. Comparison of experimental VDE and ADE values to B3LYP/def2-TZVPP calculated ones of the four lowest-energy isomers for $MFe(CO)_4^-$ (M = Si, Ge, Sn).

Cluster	Isomer	Relative energy (eV)	VDE		ADE	
			Expt.[a]	Calc.	Expt.[a]	Calc.
$SiFe(CO)_4^-$	4A	0.00	2.74 (4)	2.54	2.06 (7)	1.98
	4B	0.16		3.41		2.84
	4C	0.45		2.55		2.33
	4D	0.73		2.81		2.27
$GeFe(CO)_4^-$	4a	0.00	2.25 (6)	2.23	1.96 (8)	1.95
	4b	0.74		2.43		2.31
	4c	1.11		3.68		3.24
	4d	1.14		2.00		1.73
$SnFe(CO)_4^-$	4-I	0.00	2.12 (7)	2.14	1.88 (8)	1.95
	4-II	0.87		2.90		2.51
	4-III	0.93		2.01		1.81
	4-IV	1.44		2.38		1.77

[a]Numbers in parentheses represent the uncertainty in the last digit.

Sn) are 2.74 ± 0.04, 2.25 ± 0.06, and 2.12 ± 0.07 eV, respectively, which show a slight decrease trend with the growing atomic number.

For $SiFe(CO)_4^-$, it has a broad spectrum feature at the high binding energy side, indicating a two-photon process of $SiFe(CO)_4^-$ anion, i.e., $SiFe(CO)_4^-$ is photo-dissociated by absorbing the first photon to an excited state, and the subsequent fragment anions are then detached by the second photon. In addition, there's a higher binding energy peak next to the dominant peak, located at 3.00 eV. $GeFe(CO)_4^-$ and $SnFe(CO)_4^-$ also have higher binding energy peaks; to be specific, 2.60 and 2.90 eV for $GeFe(CO)_4^-$, and 2.60 and 3.30 eV for $SnFe(CO)_4^-$. The higher the binding energy peak is located, the deeper the molecular orbital the electron gets detached from.[37] While the ground-state adiabatic detachment energy (ADE) could not be obtained directly because of the lack of vibrational information, it can be estimated by drawing a line at the leading edge of the VDE peak and adding the instrumental resolution to the crossing point between the line and x-axis. The ADE values of $MFe(CO)_4^-$ (M = Si, Ge, Sn) are estimated to be 2.06 ± 0.07, 1.96 ± 0.08, and 1.88 ± 0.8 eV, respectively.

B. Identification of geometric structure

To elucidate the geometric structures of each species on the basis of the experimental results, the quantum chemical calculations were carried out for $MFe(CO)_4^-$ (M = Si, Ge, Sn). The possible structures have been tried, and their geometries and energies are shown in Figs. S1–S3. For convenience, only four lowest-energy isomers for $MFe(CO)_4^-$ (M = Si, Ge, Sn) have been chosen for detailed debating in the text. The experimental and calculated VDEs/ADEs are listed in Table I. The optimized structures and their relative energies are displayed in Fig. 2.

$SiFe(CO)_4^-$. The most stable structure of $SiFe(CO)_4^-$, shown in Fig. 2 and labeled as 4A, has a $^2B_2$ ground state and the C_{2v} symmetry, with four terminal CO all coordinating to the Fe center. The calculated VDE and ADE of 4A are 2.54 and 1.98 eV, respectively, which reasonably agree with the experimental results (2.74 ± 0.04 and 2.06 ± 0.07 eV). The next lowest-lying isomer 4B, in which CO, SiO, and C_3O_2 are bonded to the Fe atom, has a plane structure with a $^2A'$ electronic state. C_3O_2 is a bidentate ligand, with two carbon atoms coordinating with an iron atom. 4B is 0.16 eV higher in energy than 4A. The VDE and ADE by theoretical prediction are 3.41 and 2.84 eV, respectively, both of which are not in accord with the experimental values. Similar to 4B, the isomer 4C also has C_s symmetry but is 0.45 eV less stable than 4A. In 4C, three carbonyl and SiCO ligands coordinate with the metal center by the end-on pattern. The theoretical values of VDE and ADE of 4C are 2.55 and 2.33 eV, respectively, both of which fit with experiments. However, considering its energy, its existence under the experimental conditions could be completely excluded. The isomer 4D could be regarded as the excited state of 4B and possesses a ^4A state, which lies 0.73 eV above 4A. The computed VDE and ADE of 4D are 2.81 and 2.27 eV, respectively, which conform to experimental values nicely. However, like 4C, the high energy of 4D hinders its formation in the experiments. Therefore, we can identify the isomer 4A as the true structure of the $SiFe(CO)_4^-$ cluster.

$GeFe(CO)_4^-$. The lowest-lying isomer structure of $GeFe(CO)_4^-$, shown in Fig. 2 and labeled as 4a, also has a $^2B_2$ ground state, whose structure is similar to 4A of $SiFe(CO)_4^-$. The calculated VDE and ADE of 4a are 2.23 and 1.95 eV, respectively, which agree well with the experimental results (2.25 ± 0.06 and 1.96 ± 0.08 eV). Meanwhile, 4b is analogous to 4C and 0.74 eV higher in energy than 4a. For 4c, two CO and one bidentate OCCGeO ligands are bonded to the Fe atom, which has a $^2A'$ state and is 1.11 eV higher in energy than 4a. 4d could be deemed the excited state of 4a, which has the $^4A'$ state and lies 1.14 eV higher in energy than 4a. The calculated VDEs/ADEs of isomer 4b–4d are 2.43/2.31, 3.68/3.24, and 2.00/1.73 eV, respectively. The isomers 4b and 4d are well consistent with the experimental values, but 4c is not. Nevertheless, the excessive energies compared with 4a lead to the impossibility of the existence of 4b–4d. Therefore, isomer 4a contributes to the experiments.

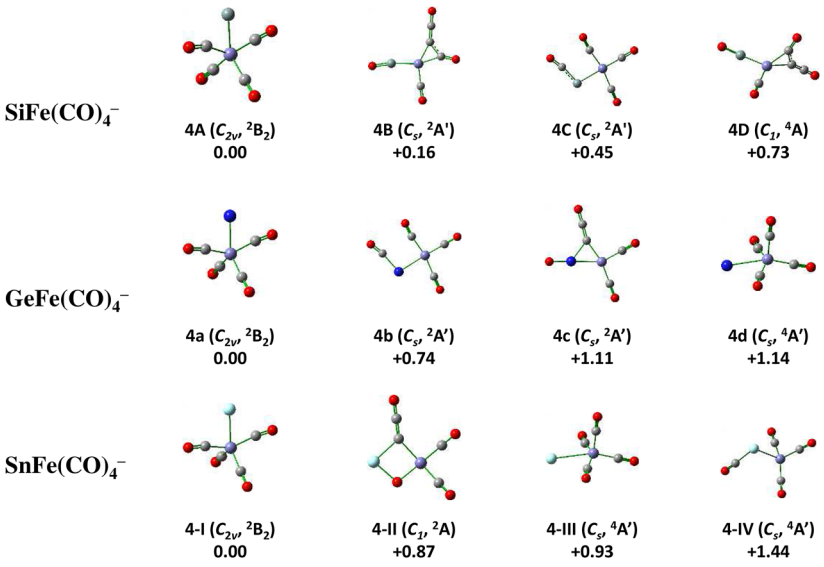

FIG. 2. Ground-state structures and selected lowest-energy isomers for $MFe(CO)_4^-$ (M = Si, Ge, Sn) (Si, cadet blue; Ge, blue; Sn, aquamarine; Fe, purple; C, gray; O, red) anions calculated at the B3LYP/def2-TZVPP level.

$SnFe(CO)_4^-$. The most stable isomer of $SnFe(CO)_4^-$ is shown in Fig. 2 and labeled as 4-I. Similar to 4A and 4a, it still has a $^2B_2$ ground state and the C_{2v} symmetry. In 4-II, one CCO and O atom bridge with Fe and Sn atoms, and the other two CO ligands terminally interact with metal atoms, which have a ^2A state and lie 0.87 eV higher in energy than 4-I. 4-II is similar to 4d, and its energy increases by 0.93 eV relative to 4-I. For 4-IV, three CO molecules are bonded to Fe, while one CO coordinates with Sn. It has a $^4A'$ state and is 1.44 eV less stable than 4-I. The calculated VDE and ADE of 4-I are 2.12 and 1.95 eV, which are in good agreement with the experimental results (2.12 ± 0.07 and 1.88 ± 0.08 eV). Meanwhile, the VDEs/ADEs of isomers 4-II, 4-III, and 4-IV are predicted to be 2.90/2.51, 2.01/1.81, and 2.38/1.77 eV, respectively. The isomers 4-III and 4-IV have good agreements with experimental results, but 4-II do not. However, as high energy isomers, it is difficult for them to be produced in the experiments. The isomer 4-I can thus be observed in the experiments.

The rest of the high-energy isomers in Figs. S1–S3 are also unable to be produced during the experiments as discussed earlier, which could also be precluded. After the comparison between the calculational and experimental results discussed earlier, the geometric structure of $MFe(CO)_4^-$ (M = Si, Ge, Sn) can thus be identified as an M–Fe bonded, iron-center, and carbonyl-terminal anionic structure with C_{2v} symmetry, which could also be seen in the previous studies of $PbFe(CO)_4^-$.[37] Therefore, the group 14 iron tetracarbonyl clusters $MFe(CO)_4^-$ have different geometric structures with other reported carbonyl clusters $AFe(CO)_4^-$ (A = Be, Mg, Ti, V, Cr, Cu, and Ag), which have the C_{3v} symmetry.[22–26]

IV. DISCUSSIONS

For $MFe(CO)_4^-$ (M = Si, Ge, Sn) clusters, the most likely existing structure is the iron-center CO-terminal bonded motif. The length of the M–Fe bond, shown in Table II, is 2.26, 2.37, and 2.58 Å, respectively, which shows an increasing tendency. Other theoretical methods in Table SII also give similar M–Fe bond distances. The Si–Fe bond length in $SiFe(CO)_4^-$ is in accordance with the previous studies of $[(CO)_4Fe–SiCl_3]^-$ [2.2576(8) Å] and $[(CO)_4Fe–SiPyr_3]^-$ (2.2663 Å) compounds.[38] The Ge–Fe bond of $GeFe(CO)_4^-$ is a bit longer than that in K[(tmim)$GeFe(CO)_4$] [2.2978(16) Å][39] and in line with that in Digermathiirane 8 [2.3601(8) Å][40] and [EMIm][$Ge_2I_6Fe(CO)_{3I}$] (2.389 Å)[41] compounds. The sums of the singlet/double covalent bond radius of M (M = Si–Sn) and Fe recommended by Pyykkö[42,43] are 2.32/2.16, 2.37/2.20, and 2.56/2.39 Å, respectively. It indicates that Si–Fe bonds are between single and double bonds, while Ge/Sn–Fe bonds are close to single bond. Moreover, the calculated Wiberg bond orders of M–Fe (M = Si, Ge, Sn) are 0.91, 0.89, and 0.83, respectively, which suggests M–Fe bonds are all single bonds. However, Wiberg bond order is not a reliable indicator, especially for metal bonding, as previous studies reported.[44,45] The $MFe(CO)_3^-$ (M = C–Pb) species have already been determined to have a triply bonded M–Fe bond.[45] The calculated bond energies of M–Fe bonds of $MFe(CO)_3^-$ and $MFe(CO)_4^-$

TABLE II. M–Fe bond lengths, Wiberg bond orders, and natural charges of $MFe(CO)_4^-$ (M = Si, Ge, Sn) species calculated at the B3LYP/def2-TZVP level of theory.

Species	M–Fe bond length	M–Fe Wiberg bond order	Natural charge	
			M	Fe
$SiFe(CO)_4^-$	2.26	0.91	0.43	−2.29
$GeFe(CO)_4^-$	2.37	0.89	0.34	−2.34
$SnFe(CO)_4^-$	2.58	0.83	0.31	−2.35

TABLE III. Bond energies (kcal/mol) and critical point ellipticity (a.u.) of the M–Fe bond of $MFe(CO)_3^-$ and $MFe(CO)_4^-$ (M = Si, Ge, Sn) species calculated at the B3LYP/def2-TZVP level of theory.

Species	Bond energies	Critical point ellipticity
$SiFe(CO)_3^-$	87.1	0.002
$SiFe(CO)_4^-$	65.7	0.689
$GeFe(CO)_3^-$	79.5	0.001
$GeFe(CO)_4^-$	61.0	0.251
$SnFe(CO)_3^-$	65.6	0.006
$SnFe(CO)_4^-$	57.9	0.249

(M = Si–Sn) are shown in Table III, which displays that after another CO coordinate to $MFe(CO)_3^-$, bond energies of M–Fe only decrease 21.5, 18.4 and 7.7 kcal/mol for Si–Sn, respectively. Therefore, M–Fe bonds in $MFe(CO)_4^-$ are more likely doubly bonded. What is more, the critical point ellipticities of M–Fe by the quantum theory of atoms in molecules[46] of $MFe(CO)_3^-$ in Table III are close to zero, which supports triple bond assignments. While for $MFe(CO)_4^-$, the critical point ellipticities of M–Fe are obviously larger than zero, which demonstrates M–Fe are double bonds.

Moreover, the contours of the frontier molecular orbitals (MOs) of $MFe(CO)_4^-$ (M = Si, Ge, Sn) clusters are displayed in Fig. 3. The atomic orbital contributions of MOs for Si–Sn are listed in Tables SIII–SV. The singly occupied molecular orbitals (SOMO) are mainly *n*p atomic orbitals of *M*, with compositions of 50% Si 3p, 68% Ge 4p, and 81% Sn 5p, respectively. The doubly occupied HOMOs show the σ-bonding interactions between the *n*s and *n*p orbits of M atoms and the 3d and 4p orbitals of Fe atoms. It is worth mentioning that the HOMO-2 orbitals of $MFe(CO)_4^-$ are typical π back-donations from the 3d and 4p orbitals of Fe to the empty *n*p orbitals of M. The other MOs (from HOMO-3 to HOMO-5) are mainly due to interactions between Fe and CO molecules. In consequence, the M–Fe bond has one electron-sharing σ bond and one Fe → M dative π bond.

In addition, the natural charges of Fe for the three species in Table II are around −2.30, which shows that the negative charge is mainly located on Fe and is consistent with the result of their homolog $PbFe(CO)_4^-$.[37] The natural charges of the $Fe(CO)_4$ moiety for $MFe(CO)_4^-$ (M = Si, Ge, Sn) are −1.43, −1.34, and −1.31,

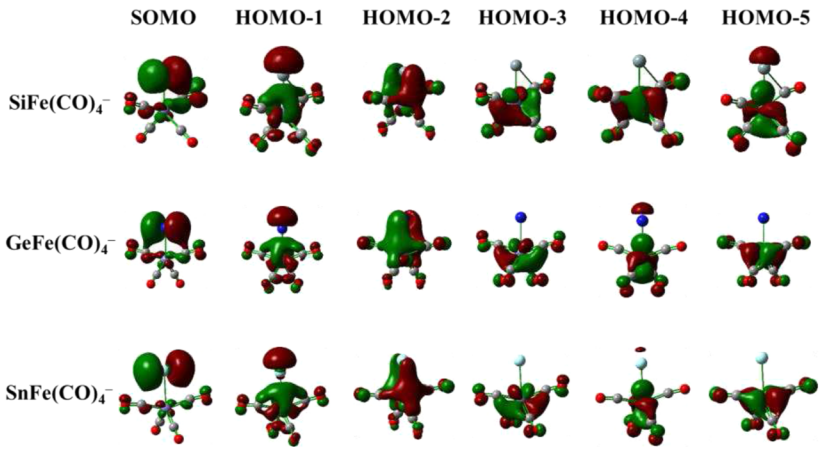

FIG. 3. Molecular orbital pictures of the most stable isomers for $MFe(CO)_4^-$ (M = Si, Ge, Sn) calculated at the RO-B3LYP/def2-TZVPP level of theory, showing the singly occupied molecular orbitals (SOMO) down to the fifth valence molecular orbital from the HOMO.

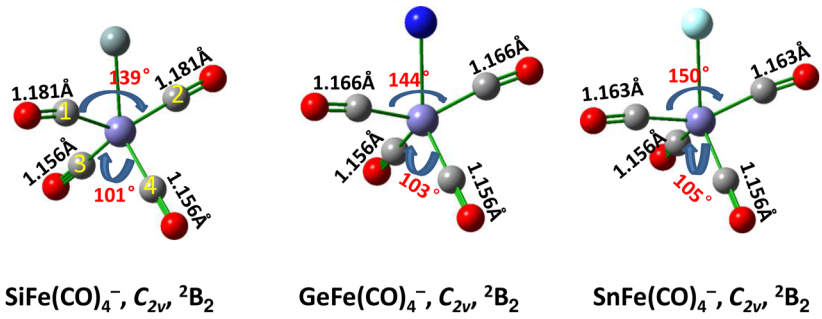

FIG. 4. The C–O bond lengths and bond angles of the lowest-energy isomers for $MFe(CO)_4^-$ (M = Si, Ge, Sn) (Si, cadet blue; Ge, blue; Sn, aquamarine; Fe, purple; C, gray; O, red) calculated at the B3LYP/def2-TZVPP level.

respectively. Therefore, $MFe(CO)_4^-$ contains the $[M]^0[Fe(CO)_4]^-$ ion core. Furthermore, the spin population analyses in Fig. S4 and Table S6 show that the unpaired electron is mainly located on M, which also supports our conclusions about the ion core and M–Fe bonds. Hence, the central Fe atom has a favorable 18-electron configuration.

As shown in Table III, with the atomic number growing, the bond energies of M–Fe bonds are reduced, which indicates the interaction between M and Fe is decreased. As shown in Fig. 4, from Si to Sn, the bond angle ∠C1–Fe–C2 grows from 139° to 150° (∠C3–Fe–C4 on the other side from 101° to 105°), while the C1–O bond decreases from 1.181 to 1.163 Å, longer than 1.13 Å in a free CO molecule. In light of the analyses above, with M changing from Si to Sn, the structure of $MFe(CO)_4^-$ is becoming loose, and the activation of CO becomes more weaker since the enlarged radius of *M* and the decreased interactions between the M and Fe.

In summary, compared with $MFe(CO)_3^-$ (M = Si, Ge, Sn) anionic clusters,[45] the extra added CO makes $MFe(CO)_4^-$ symmetry lower, and the original C_{3v} structure could not maintain any more. After becoming C_{2v} structure, the SOMO orbital of $MFe(CO)_4^-$ has the b_2 symmetry instead of a_1. So, one singly occupied *n*p atomic orbital of M will not participate in bonding. Therefore, the M and Fe atoms form double bonds in $MFe(CO)_4^-$ and Fe atom fulfills the 18-eletron count.

V. CONCLUSIONS

The anionic clusters $MFe(CO)_4^-$ (M = Si, Ge, Sn) were generated by laser ablations on M–Fe alloys and analyzed by homemade mass-photoelectron spectroscopy. Combined with quantum chemical calculations, it turns out that all the $MFe(CO)_4^-$ clusters have a $^2B_2$ ground state, the C_{2v} symmetry, and the iron-center carbonyl-terminal structure. The electronic structure analyses of $MFe(CO)_4^-$ show that M–Fe is a double bond, and the central Fe atom has the 18-electron configuration. The C–O bonds in those three anionic clusters are activated to different extents, and the C–O bond in $SiFe(CO)_4^-$ is elongated more. The Si–Fe alloy thus turns out to be a better collocation to activate the C–O bond in the gas phase. These results would advance the understanding of chemisorbed CO molecules on alloy surfaces, which can guide future catalytic design for CO resource transformation and utilization.

SUPPLEMENTARY MATERIAL

See the supplementary material for additional details of bond lengths, orbital composition analysis, unpaired spin density distributions, and optimized structures of the low-energy isomers for $MFe(CO)_4^-$ (M = Si, Ge, Sn).

ACKNOWLEDGMENTS

The authors gratefully acknowledge the Dalian Coherent Light Source (DCLS) for support and assistance. This work was supported by the National Natural Science Foundation of China (Grant Nos. 22273101, 22125303, 92061203, 22373102, and 22288201), the Youth Innovation Promotion Association of the Chinese Academy of Sciences (Grant No. 2020187), the Henan Key Scientific Research Projects (22A150001), the Dalian Young Star of Science and Technology Project (Grant No. 2021RQ128), the Dalian Institute of Chemical Physics (DICP DCLS201702), and the Strategic Priority Research Program of CAS (XDB17000000).

AUTHOR DECLARATIONS

Conflict of Interest

The authors have no conflicts to disclose.

Author Contributions

Bangmin Ju: Conceptualization (equal); Data curation (equal); Formal analysis (equal); Writing – original draft (equal). **Ziheng Zhang**: Conceptualization (equal); Data curation (equal); Formal analysis (equal); Writing – original draft (equal). **Xiangtao Kong**: Conceptualization (lead); Project administration (lead); Supervision (lead); Validation (lead); Writing – review & editing (lead). **Jinghan Zou**: Conceptualization (equal); Data curation (equal); Formal analysis (equal); Writing – original draft (equal). **Gang Li**: Conceptualization (equal); Data curation (equal); Formal analysis (equal); Writing – original draft (equal). **Hua Xie**: Conceptualization (lead); Project administration (lead); Supervision (lead); Validation (lead); Writing – review & editing (lead). **Ling Jiang**: Conceptualization (lead); Project administration (lead); Supervision (lead); Validation (lead); Writing – review & editing (lead).

DATA AVAILABILITY

The data that support the findings of this study are available from the corresponding author upon reasonable request.

REFERENCES

[1] F. A. Cotton and R. A. Walton, *Multiple Bonds between Metal Atoms* (Clarendon Press, 1993).
[2] C. E. Housecroft, *Metal–Metal Bonded Carbonyl Dimers and Clusters* (Oxford University Press, Oxford, UK, 1996).
[3] B. Yoon, H. Häkkinen, U. Landman, A. S. Wörz, J. M. Antonietti, S. Abbet, K. Judai, and U. Heiz, Science **307**, 403 (2005).
[4] C. Burgel, N. M. Reilly, G. E. Johnson, R. Mitric, M. L. Kimble, A. W. Castleman, and V. Bonacic-Koutecky, J. Am. Chem. Soc. **130**, 1694 (2008).
[5] S. M. Lang and T. M. Bernhardt, Phys. Chem. Chem. Phys. **14**, 9255 (2012).
[6] M. Cargnello, V. V. T. Doan-Nguyen, T. R. Gordon, R. E. Diaz, E. A. Stach, R. J. Gorte, P. Fornasiero, and C. B. Murray, Science **341**, 771 (2013).
[7] H. Schwarz, Angew. Chem., Int. Ed. **54**, 10090 (2015).
[8] L. S. Chen, J. J. Chen, T. M. Ma, X. N. Li, and S. G. He, Chem. Phys. Lett. **787**, 139276 (2022).
[9] K. T. Rommens and M. Saeys, Chem. Rev. **123**, 5798 (2023).
[10] R. A. J. O'Hair and G. N. Khairallah, J. Cluster Sci. **15**, 331 (2004).
[11] W. Xue, Z. C. Wang, S. G. He, Y. Xie, and E. R. Bernstein, J. Am. Chem. Soc. **130**, 15879 (2008).
[12] S. G. Ard, O. Martinez, S. A. Brown, J. C. Sawyer, P. B. Armentrout, A. A. Viggiano, and N. S. Shuman, Phys. Chem. Chem. Phys. **19**, 8768 (2017).
[13] R. D. Ernst, T. J. Marks, and J. A. Ibers, J. Am. Chem. Soc. **99**, 2090 (1977).
[14] R. D. Ernst and T. J. Marks, Inorg. Chem. **17**, 1477 (1978).
[15] C. B. Lagrone, K. H. Whitmire, M. R. Churchill, and J. C. Fettinger, Inorg. Chem. **25**, 2080 (1986).

[16]K. H. Whitmire, C. B. Lagrone, M. R. Churchill, J. C. Fettinger, and B. H. Robinson, Inorg. Chem. **26**, 3491 (1987).
[17]H. Schwarz, Catal. Sci. Technol. **7**, 4302 (2017).
[18]P. Ferrari, J. Vanbuel, E. Janssens, and P. Lievens, Acc. Chem. Res. **51**, 3174 (2018).
[19]Y. X. Zhao, Z. Y. Li, Y. Yang, and S. G. He, Acc. Chem. Res. **51**, 2603 (2018).
[20]X. N. Li, L. N. Wang, L. H. Mou, and S. G. He, J. Phys. Chem. A **123**, 9257 (2019).
[21]L. Mond and C. Langer, J. Chem. Soc., Trans. **59**, 1090 (1891).
[22]N. Zhang, M. B. Luo, C. X. Chi, G. J. Wang, J. M. Cui, and M. F. Zhou, J. Phys. Chem. A **119**, 4142 (2015).
[23]Z. L. Liu, Y. Bai, Y. Li, J. He, Q. Y. Lin, L. N. Hou, H. S. Wu *et al.*, Dalton Trans. **49**, 15256 (2020).
[24]G. J. Wang, J. Zhao, H. S. Hu, J. Li, and M. F. Zhou, Angew. Chem., Int. Ed. **60**, 9334 (2021).
[25]J. M. Zhang, Z. L. Liu, G. Li, H. J. Fan, L. Jiang, and H. Xie, J. Energy Chem. **63**, 344 (2021).
[26]X. Y. Jin, G. J. Wang, and M. F. Zhou, Phys. Chem. Chem. Phys. **25**, 7697 (2023).
[27]C. X. Chi, H. Qu, L. Y. Meng, F. C. Kong, M. B. Luo, and M. F. Zhou, Angew. Chem., Int. Ed. **56**, 14096 (2017).
[28]Z. B. Qin, X. Wu, and Z. C. Tang, Rev. Sci. Instrum. **84**, 066108 (2013).
[29]V. Dribinski, A. Ossadtchi, V. A. Mandelshtam, and H. Reisler, Rev. Sci. Instrum. **73**, 2634 (2002).
[30]M. J. Frisch, G. W. Trucks, H. B. Schlegel, G. E. Scuseria, M. A. Robb, J. R. Cheeseman, G. Scalmani, V. Barone, G. A. Petersson, H. Nakatsuji, X. Li, M. Caricato, A. V. Marenich, J. Bloino, B. G. Janesko, R. Gomperts, B. Mennucci, H. P. Hratchian, J. V. Ortiz, A. F. Izmaylov, J. L. Sonnenberg, D. Williams-Young, F. Ding, F. Lipparini, F. Egidi, J. Goings, B. Peng, A. Petrone, T. Henderson, D. Ranasinghe, V. G. Zakrzewski, J. Gao, N. Rega, G. Zheng, W. Liang, M. Hada, M. Ehara, K. Toyota, R. Fukuda, J. Hasegawa, M. Ishida, T. Nakajima, Y. Honda, O. Kitao, H. Nakai, T. Vreven, K. Throssell, J. A. Montgomery, Jr., J. E. Peralta, F. Ogliaro, M. J. Bearpark, J. J. Heyd, E. N. Brothers, K. N. Kudin, V. N. Staroverov, T. A. Keith, R. Kobayashi, J. Normand, K. Raghavachari, A. P. Rendell, J. C. Burant, S. S. Iyengar, J. Tomasi, M. Cossi, J. M. Millam, M. Klene, C. Adamo, R. Cammi, J. W. Ochterski, R. L. Martin, K. Morokuma, O. Farkas, J. B. Foresman, and D. J. Fox, *GAUSSIAN 09 Rev. A.02*, Wallingford, CT, Wallingford, 2016.
[31]P. J. Stephens, F. J. Devlin, C. F. Chabalowski, and M. J. Frisch, J. Phys. Chem. **98**, 11623 (1994).
[32]A. D. Becke, J. Chem. Phys. **98**, 5648 (1993).
[33]C. Lee, W. Yang, and R. G. Parr, Phys. Rev. B **37**, 785 (1988).
[34]F. Weigend and R. Ahlrichs, Phys. Chem. Chem. Phys. **7**, 3297 (2005).
[35]T. Lu and F. W. Chen, J. Comput. Chem. **33**, 580 (2012).
[36]A. E. R. E. D. Glendening, J. E. Carpenter, and F. Weinhold, *NBO Version 3.1*, 2016.
[37]Z. L. Liu, J. H. Zou, Z. Qin, H. Xie, H. J. Fan, and Z. C. Tang, J. Phys. Chem. A **120**, 3533 (2016).
[38]L. Witteman, M. Lutz, and M. E. Moret, Organometallics **37**, 3024 (2018).
[39]L. Witteman, C. B. van Beek, O. N. van Veenhuizen, M. Lutz, and M.-E. Moret, Organometallics **38**, 231 (2019).
[40]A. Jana, V. Huch, H. S. Rzepa, and D. Scheschkewitz, Organometallics **34**, 2130 (2015).
[41]S. Wolf, A. Egeberg, J. Treptow, and C. Feldmann, Chemistryopen **10**, 171 (2021).
[42]P. Pyykko and M. Atsumi, Chem. - Eur. J. **15**, 12770 (2009).
[43]P. Pyykko and M. Atsumi, Chem. - Eur. J. **15**, 186 (2009).
[44]J. Q. Wang, C. Chi, H. S. Hu, L. Y. Meng, M. B. Luo, J. Li, and M. F. Zhou, Angew. Chem., Int. Ed. **57**, 542 (2018).
[45]J. Q. Wang, C. X. Chi, J. B. Lu, L. Y. Meng, M. B. Luo, H. S. Hu, M. Zhou, and J. Li, Chem. Commun. **55**, 5685 (2019).
[46]B. E. Atkinson, H. S. Hu, and N. Kaltsoyannis, Chem. Commun. **54**, 11100 (2018).